ELSEVIER

Nuclear Instruments and Methods in Physics Research B 166–167 (2000) 451–458

NIM B
Beam Interactions with Materials & Atoms

www.elsevier.nl/locate/nimb

Self-trapped excitons in quartz

Jakyoung Song [a,b], Hannes Jónsson [b], L. René Corrales [a,*]

[a] *Environmental Molecular Science Laboratory, Pacific Northwest National Laboratory, P.O. Box 999, MS K8-91, 902 Batelle Blvd., Richland, WA 99352, USA*

[b] *Department of Chemistry, University of Washington, Seattle, WA 98195, USA*

Abstract

Triplet-state electronic excitations in quartz were studied using density functional theory (DFT). By using periodic boundary conditions, the lattice response and electronic structure relaxations can be determined in the bulk. Several self-trapped exciton (STE) states have been discovered, in addition to the oxygen-distorted state, which was originally predicted 10 years ago. One of these states is a silicon-distorted state that lies energetically close to the oxygen-distorted state. The results reveal that these two major STE states are likely responsible for two distinct luminescence bands. The luminescence energies for STE states of impurities and intrinsic defects were also determined.

Keywords: Self-trapped excitons; Quartz; Density functional theory

1. Introduction

When quartz is exposed to a low flux of ionizing radiation, self-trapped excitons (STEs) are formed [1]. Several luminescence peaks are observed for the decay of STEs, with a strong Stokes' shift from the original absorption peak. Despite, extensive experimental studies to characterize the luminescence spectra of quartz [2–9], the assignments are not well understood. Some of the spectral peaks have been assigned to extrinsic defects. Other peaks are likely due to STE state(s) and intrinsic defects. It has been long believed that the self-trapping mechanism of an exciton in quartz was due to an oxygen distortion [10]. This was based on previous cluster calculations of an STE state in quartz by Fisher et al. [11] that revealed a self-trapping mechanism involving a lattice distortion to form an oxygen-distorted state. However, cluster calculations cannot reveal the role and response of the lattice in the presence of electronic excitations. Thus, alternative theoretical methods are needed to determine the lattice relaxation and electronic structural rearrangement in the bulk structure.

In this work, triplet-excited electronic states in crystalline quartz have been calculated using density functional theory (DFT) in a plane wave code. A distinct advantage of DFT is that calculations can be carried out for a 72-atom system using periodic boundary conditions. In this way, the

* Corresponding author. Tel.: +1-509-376-6608; fax: +1-509-376-0420.

E-mail address: rene.corrales@pnl.gov (L.R. Corrales).

0168-583X/00/$ - see front matter
PII: S0168-583X(99)00785-5

structural response of the lattice to the excitation is captured in significant detail. For example, the excitations can lead to structures where a silicon atom forms a backbond with an oxygen atom. In order to capture these kind of effects, a cluster model would need to include a larger number of atoms. These backbonds are precisely like those for the E' oxygen vacancy center calculated by Fowler et al. [12].

Several intrinsic STE states have been found in quartz, some of which are significantly higher in energy than others. The oxygen-distorted STE is found to be the most stable state relative to other STE states. However, nearby is a silicon-distorted state that is only 0.23 eV higher in energy. This STE displays significantly larger broken bond character than the oxygen-distorted STE and, consequently, has a larger volume change in its formation. Moreover, this work shows that these two important STE states have luminescence bands that are widely separated.

DFT cannot be expected to give accurate luminescence energies. But, it is interesting to study trends in going from pure quartz to impurities in quartz to compare with wave function ab initio calculations and experiment. We have examined the triplet excited states of Ge [13] and Al [14,15] impurities as well as interstitial [16], vacancy [17–20] and a Frenkel pair defect [21,22] of quartz. This allows a direct comparison of the emission energies of the triplet (excited) to singlet (ground) state of each of the defect and impurity structures for both the oxygen and silicon distorted STEs.

2. Theoretical approach: DFT

In this work, the DFT calculations were carried out using VASP [23–26] (Vienna ab initio simulation program). VASP is a plane wave DFT code based on local-density approximation (LDA) and generalized gradient corrections (GGC) using the Perdew–Wang 91 functional. In addition, the ultrasoft Vanderbilt pseudopotential (USPP) and spin polarization were used. The energy cutoffs were 29 Ry for the wave functions and 68 Ry for the augmented electron density. The Brillouin zone of the cell was sampled only at the Γ-point. The system consisted of 72 atoms made up of 24 silicon and 48 oxygen atoms in a periodic orthorhombic cell. Optimization of the structures was carried out using an iterative conjugate gradient minimization scheme.

3. Results: STEs

The starting configuration is a perfect crystal lattice of quartz as determined by experiment and is shown in Fig. 1(a). The lattice constant obtained after relaxing the configuration using DFT is within 1% of the experimental lattice constant. The initial triplet-state excitation in the perfect lattice leads to the delocalization of both the excited electron and the valence hole. This will be referred to as the free exciton (FE) state. The delocalization of the electron–hole pair over the entire system is likely due to the small system size. In a real system the delocalization is expected to be over a small region of the bulk material. Shown in Fig. 1(b) is the spin density difference of excess spin-up, the gray region, and excess spin-down, the green region. These were calculated using density cutoffs of 0.33 e and −0.01 e, respectively. The spin density differences effectively indicate the locations of the valence-hole (gray region) and excited-electron (green region). An analysis of orbital occupation reveal that the valence-hole is effectively delocalized in the molecular orbital (MO) made up of the lone-pair p orbitals of the oxygen atoms, and that the excited electron is effectively delocalized on the MO made up of the 4 s orbitals of the silicon atoms.

The oxygen-distorted state is obtained by pushing an oxygen atom perpendicular to its bonds. This structure is then allowed to relax both its electronic and ionic configurations to the nearest minimum, shown in Fig. 2(a). In the end, three oxygen atoms have moved in a similar way, indicated by the arrows in Fig. 2(a). The spin density difference shown in Fig. 2(b) has been used to verify that this is a localized exciton state.

The orbital analysis shows that the valence-hole is occupying a MO that is effectively made up of the lone-pair orbitals of the three oxygen atoms.

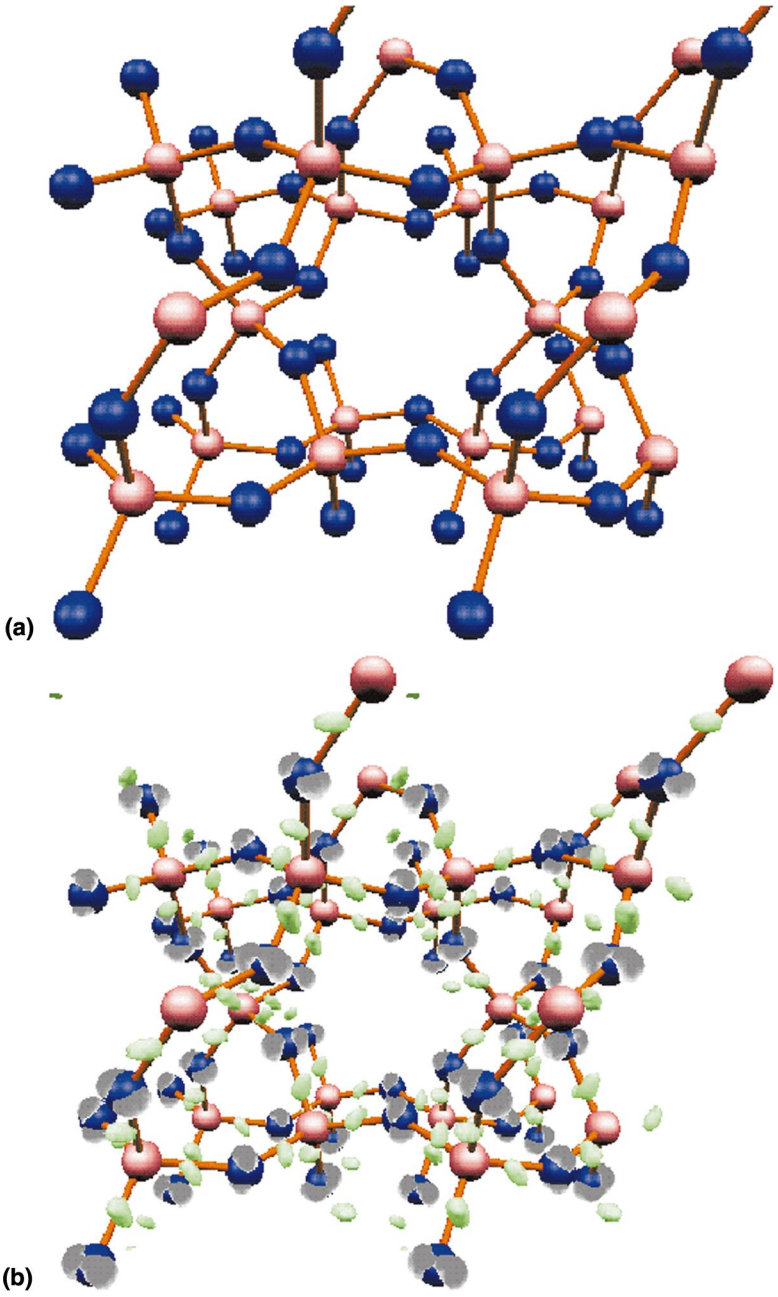

Fig. 1. (a) The perfect quartz lattice. The silicon atoms are red and the oxygen atoms are blue. (b) The spin densities due to the excited electron (green) and the valence-hole (gray). Both the excited electron and valence-hole are delocalized throughout the simulation cell.

The excited-electron is effectively localized on the anti-bonding MO of the SiO bond. In contrast to the FE state of the perfect crystal, the MOs in the conduction band have swapped such that the anti-bonding MO has a lower energy in the oxygen-distorted state than in the perfect lattice.

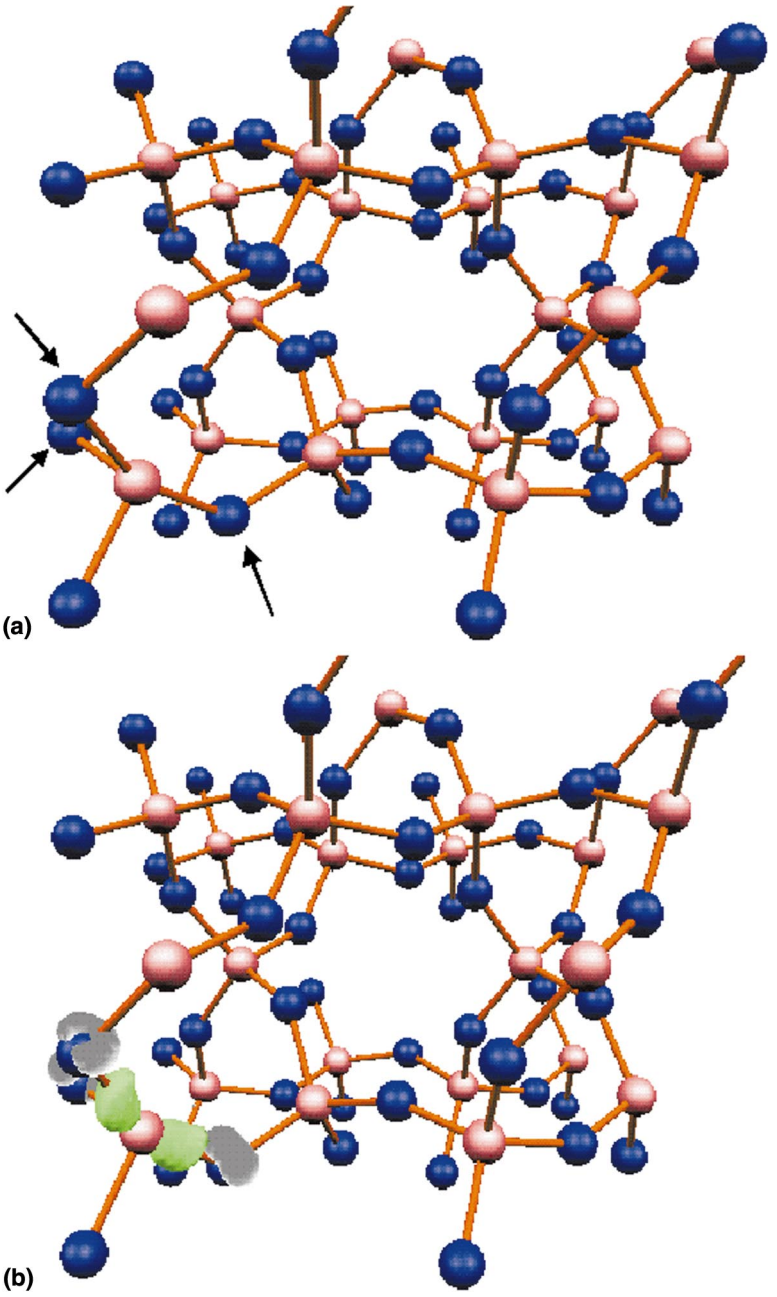

Fig. 2. The oxygen-distorted STE state. (a) The Si–O–Si bonds in the lower left portion of the configuration have been distorted with three oxygen atoms moving approximately 0.08 nm from their original position. (b) The spin density. It illustrates the localization of the STE. The gray is the spin density difference of excess spin-up and the green is of excess spin-down. The spin density differences effectively indicate the locations of the valence-hole (gray region) and excited-electron (green region).

The silicon-distorted state was found by pushing a silicon atom along one of its bonds. The system was then allowed to relax both its electronic and ionic configurations. One of the SiO bonds is sufficiently stretched to have effectively broken its bond, as shown in Fig. 3(a). This silicon forms a backbond with an oxygen forming a structure that is very similar to the backbonded structure [12] of the charged oxygen vacancy, or E' center. The spin densities were also determined as above. It was found that the excited electron and hole are localized over two sites as shown in Fig. 3(b).

In this case, the orbital analysis is more difficult to interpret. It shows that the valence-hole is localized on the lone-pairs of the oxygen with the broken bond and apparently also on the backbonded oxygen. The excited-electron is localized on the anti-bonding MOs of three SiO bonds belong to the silicon with a broken bond and a backbond, as well as on the remaining SiO bond of the oxygen with the broken bond.

The absorption energy E_a is the energy to promote an electron from the top of the valence band to the bottom of conduction band and is therefore correlated with the band gap. The band gap determined for SiO_2 is 6.1 eV, consistent with other DFT calculations [27], but certainly not in agreement with wave function ab initio methods [28–30]. As stated above, DFT cannot be expected to give accurate luminescent energies, in particular because it cannot be expected to give accurate band gap energies. After introducing the excitation, the system is allowed to find a lower energy state as described above. The lattice relaxation energy E_{lr} is the energy difference between the perfect crystal excited state, the FE state, and the relaxed distorted excited states. Here again, the lattice relaxation energies cannot be expected to be accurate using DFT. The luminescence (or emission) energy E_e of the distorted states was determined by taking the relaxed excited state configuration and calculating the ground state energy on this fixed geometry. The system was then allowed to relax in the ground state to determine if it went back to the perfect crystalline state. In both cases they did. The non-radiative decay energy E_{nr} was then determined by taking the difference of the unrelaxed ground state energy and the perfect crystal state energy. These energies are shown in Table 1. The parenthesis indicates that E_{lr} is actually uphill in energy for both distorted states with respect to the FE state. This is contrary to results of small cluster Hartree–Fock ab initio calculations of Fisher et al. [11] and it may be due to DFT favoring delocalized states. In contrast, the Hartree–Fock method favors localized states.

The emission energies were determined for the Ge and Al impurities, and are shown in Table 2. The Ge impurity has two STE states similar to those found for pure SiO_2. The O-distorted state has emission energy of 2.61 eV and the Ge-distorted state has emission energy of 0.2 eV. Both show a red shift from the pure SiO_2 state, in qualitative agreement with that observed by experiment [13]. In this work, the Al impurity, that is charge compensated by a H^+, has a tetrahedrally coordinated Al, where one of the coordinating oxygen atoms is also coordinated by the hydrogen atom. This particular structure does not show a STE state and no Stoke's shift is predicted. In contrast, experiment [31] predicts an emission energy of 3.12 eV associated with a STE.

The emission energies of some intrinsic defects of quartz were also determined. The defect states included the neutral and positively charged (E'_1 center) oxygen vacancy, the neutral (peroxy linkage) and charged (peroxy radical) oxygen interstitial, and the Frenkel pair formed by the neutral oxygen vacancy and neutral oxygen (peroxy linkage) interstitial. These energies are shown in Table 3. It is interesting to note that the peroxy linkage by itself does not show a STE state. Upon excitation it dissociates and then upon de-excitation it returns to the original configuration with negligible emission energy. In contrast, the peroxy linkage that is part of the neutral Frenkel pair dissociates upon introducing the triplet excitation and forms a STE. There are two geometric configurations of the Frenkel pair peroxy linkage that are 0.1 eV in energy apart. The excited state structure of each configuration is such that the O–O bond of the peroxy linkage breaks, but the resulting structure is different in both cases.

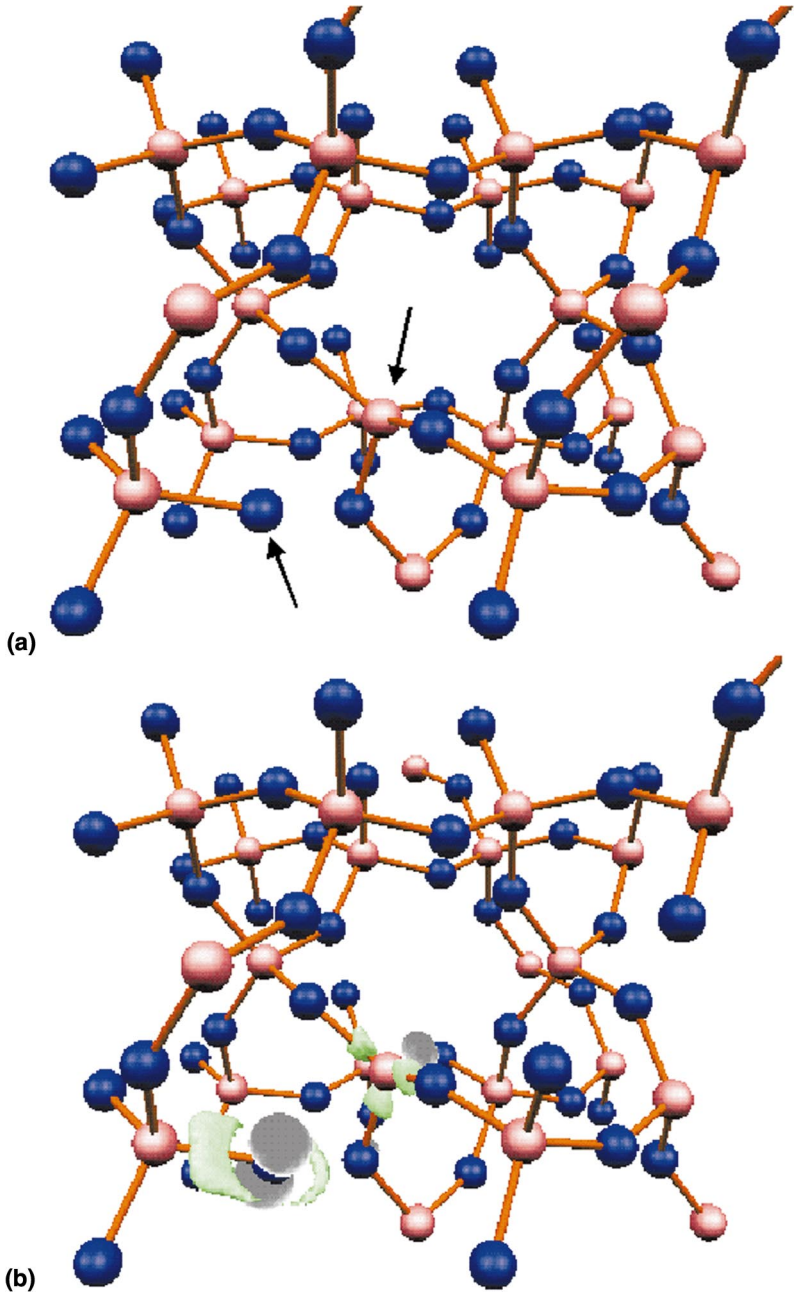

Fig. 3. The silicon-distorted STE state. (a) The Si–O bond in the lower left portion of the configuration is stretched and effectively broken with the silicon atom moving 0.084 nm from its original position. (b) The figure shows the spin density. It illustrates the localization of the STE. The gray is the spin density difference of excess spin-up and the green is of excess spin-down. The spin density differences effectively indicate the locations of the valence-hole (gray region) and excited-electron (green region). Note that the localization occurs at two sites, showing strong electronic correlation of the STE.

Table 1
Energies of STE states (in eV)[a]

	E_a	E_{lr}	E_e	E_{nr}
Perfect crystal	6.1	0	–	0
O-distorted	6.0	(0.47)	3.72	2.50
Si-distorted	6.0	(0.70)	0.90	4.70

[a] Parentheses indicate an opposite sign.

Table 2
Emission energies of impurity states (in eV)

Impurity	DFT (this work)	Experiment	Reference
Ge	2.61, 0.20	2.5	[13]
AlH	5.52	3.12	[31]
E_1' center	3.12	2.72	[31]

For the lower energy (stable) peroxy configuration, the STE structure is just like that of the O-distorted STE. For the higher energy (meta-stable) peroxy configuration, the STE structure forms a fivefold coordinated Si. When both relaxed excited state configurations are taken back to the ground state, they converge to the ideal crystal state. It is important to note that the STE state of the stable neutral Frenkel pair is lower in energy than its initial ground state configuration. However, the STE state for the meta-stable neutral Frenkel pair is higher in energy than its initial ground state configuration. These are reflected in E_{lr} of the Frenkel pairs in Table 3.

4. Discussion

The emission energies of the two STE distorted states appear to be widely separated. This may indicate that they contribute to two distinct luminescence energies. In addition, the emission energies for the intrinsic defects also show that they may contribute to distinct bands that overlap those of the STE distorted states. These calculations are currently being supplemented by ab initio and modified DFT methods to test the results presented here. It does appear that there are at least two, and possibly more, STE states responsible for luminescence. This is consistent with observations of broad bands centered at different energies [1].

The fact that more than one STE state has been found indicates that the formation of defect pairs from these states is more complex than previously thought. Our efforts to find the transition(s) from the STE states to a defect pair state are continuing. In order to find new mechanisms, it is important to use a technique that does not require knowledge of the final state. An algorithm has been recently introduced which does not require knowledge of the final state [32]. This new method is analogous to the mode-following methods frequently used in computational chemistry, but it does not require second derivatives of the energy and can thus be used in conjunction with DFT plane wave calculations.

5. Conclusion

The observed luminescent bands due to the STE states as well as to intrinsic and extrinsic

Table 3
Energies of excited defect states (in eV)

Defect state	E_a	E_{lr}	E_e	E_{nr}
Neutral vacancy	5.73	2.14	1.09	2.50
+1 Charged vacancy (E_1')	4.91	0.33	3.12	1.46
O–O peroxy linkage (neutral)	3.62	2.29	–	1.33
O–O peroxy radical (+1 charge)	5.77	0.91	4.14	0.72
Stable neutral Frenkel pair	3.33	3.88	3.72	3.00
Meta-stable neutral Frenkel pair	4.12	2.50	0.95	8.05

defects have been characterized with a DFT plane wave calculation. We have found evidence for the existence of more than one STE in quartz. In particular, a self-trapped exciton with a broken SiO bond has been identified. The energy of this broken bond configuration lies close to the state originally believed to be the single important precursor to defect pair formation. The existence of additional STEs opens the possibility of alternative mechanisms for defect pair formation.

Acknowledgements

The DFT calculations have been performed using the ab initio total energy and molecular dynamics program VASP (Vienna ab-initio simulation program) developed at the Institut für Theoretische Physik of the Technische Universität Wien [19]. This work was supported by (J.S.) the Environmental Management Science Program, Office of Environmental Management, US Department of Energy, and (L.R.C.) the Division of Chemical Sciences, Office of Basic Energy Sciences, Department of Energy. The calculations were carried out on a parallel IBM-SP computer at the William R. Wiley Environmental Molecular Sciences Laboratory, a national scientific user facility sponsored by the Department of Energy, Office of Biological and Environmental Research and located at Pacific Northwest National Laboratory. Pacific Northwest Laboratory is operated for the Department of Energy by Battelle.

References

[1] D.L. Griscom, Proceeding of the 33rd Frequency Control Symposium Electronics Industries Assn., Washington, DC, 1979, p. 98.
[2] K. Tanimura, T. Tanaka, N. Itoh, Phys. Rev. Lett. 51 (1983) 423.
[3] W. Hayes, M.J. Kane, O. Salminen, R.L. Wood, S.P. Doherty, J. Phys. C 17 (1984) 2943.
[4] N. Itoh, K. Tanimura, C. Itoh, in: R.A.B. Devine (Ed.), The Physics and Technology of Amorphous SiO_2, Plenum, New York, 1988, p. 135.
[5] C. Itoh, K. Tanimura, N. Itoh, M. Itoh, Phys. Rev. B 39 (1989) 11183.
[6] T.E. Tsai, D.L. Griscom, Phys. Rev. Lett. 67 (1991) 2517.
[7] M.A. Stevens Kalceff, M.R. Phillips, Phys. Rev. B 52 (1995) 3122.
[8] K. Shimakawa, A. Kolobov, S.R. Elliott, Adv. Phys. 44 (1995) 47.
[9] K.S. Song, R.T. Williams, Self-Trapped Excitons, Springer, New York, 1996.
[10] A.N. Trukhin, J. Non-Cryst. Solids 149 (1992) 32.
[11] A.J. Fisher, W. Hayes, A.M. Stoneham, Phys. Rev. Lett. 64 (1990) 2667.
[12] W.B. Fowler, A.H. Edwards, J. Non-Cryst. Solids 222 (1997) 33.
[13] W. Hayes, T.J.L. Jenkins, J. Phys. C 21 (1988) 2391.
[14] J.A. Weil, Radiat. Eff. 26 (1975) 261.
[15] F. Sim, C.R.A. Catlow, M. Dupuis, J.D. Watts, J. Chem. Phys. 95 (1991) 4215.
[16] V.O. Sokolov, A.B. Sulimov, Phys. Stat. Sol. B 142 (1987) K7.
[17] V.O. Sokolov, V.B. Sulimov, Phys. Stat. Sol. B 135 (1986) 369.
[18] A.H. Edwards, W.B. Fowler, J. Phys. Chem. Solids 46 (1985) 841.
[19] G. Pacchioni, G. Ieranó, Phys. Rev. Lett. 79 (1997) 753.
[20] C.M. Carbonaro, V. Fiorentini, S. Massidda, J. Non-Cryst. Solids 221 (1997) 89.
[21] W. Hayes, M.J. Kane, O. Salminen, R.L. Wood, S.P. Doherty, J. Phys. C 17 (1984) 2943.
[22] A. Shluger, E. Stefanovich, Phys. Rev. B 42 (1990) 9664.
[23] G. Kresse, J. Hafner, Phys. Rev. B 47 (1) (1993) 558.
[24] G. Kresse, J. Hafner, Phys. Rev. B 49 (1994) 14251.
[25] G. Kresse, J. Furthmüller, Comput. Math. Sci. 6 (1996) 15.
[26] G. Kresse, J. Furthmüller, Phys. Rev. B 54 (16) (1996) 11169.
[27] Y. Xu, W.Y. Ching, Phys. Rev. B 44 (1991) 11048.
[28] J.R. Chelikowsky, M. Shlüter, Phys. Rev. B 15 (1977) 4020.
[29] S.T. Pantelides, in: S.T. Pantelides (Ed.), The Physics and Chemistry of SiO_2 and its Interfaces, Pergamon, New York, 1978, p. 80.
[30] R. Dovesi, C. Pisani, C. Roetti, J. Chem. Phys. 86 (1987) 6967.
[31] M.A. Stevens Kalceff, M.R. Phillips, Phys. Rev. B 52 (1995) 3122.
[32] G. Henkelman, H. Jonsson, J. Chem. Phys. 111 (1999) 7010.